



## Preparation and amino modification of mesoporous carbon from bagasse via microwave activation and ethylenediamine polymerization for Pb(II) adsorption

Kunquan Li<sup>a,\*</sup>, Jun Li<sup>b</sup>, Mingzhou Lu<sup>a</sup>, Hua Li<sup>a,\*</sup>, Xiaohua Wang<sup>a</sup>

<sup>a</sup>College of Engineering, Nanjing Agricultural University, Nanjing 210031, China, Tel. +86 25 58606592; Fax: +86 25 58606573; email: 531700023@qq.com (K. Li), Tel./Fax: +86 25 58606573, email: lmz@njau.edu.cn (M. Lu), Tel./Fax: +86 25 58606592; email: kqlee@njau.edu.cn (H. Li), Tel. +86 25 58606574; Fax: +86 25 58606573; email: xhwang@njau.edu.cn (X. Wang)

<sup>b</sup>School of Environmental Science and Engineering, Zhejiang Gongshang University, Hangzhou, Zhejiang 310012, China, Tel. +86 25 58606574; Fax: +86 25 58606573; email: lijun681116@sina.com

Received 3 August 2015; Accepted 28 December 2015

### ABSTRACT

Bagasse mesoporous carbon (MC) was designed using an L<sub>9</sub> (3<sup>4</sup>) orthogonal experiment and then modified as a cost-effective adsorbent for Pb(II) via nitric acid oxidation and ethylenediamine polymerization. X-ray photoelectron spectroscopy (XPS) and FTIR analyses indicated that amino groups were successfully introduced into the MC after modification. Pore characterization showed that the modified carbon maintained high mesoporosity. The adsorption behavior of Pb(II) and its associated factors including pH, initial concentration, adsorbent dose, temperature, and contact time were further investigated. Results proved that the modified carbon showed excellent Pb(II) adsorption performance, which could be due to the large number of mesopores and introduced amino groups. The adsorption capacity also increased with increasing solution temperature and reached the maximum adsorption amount of 185 mg g<sup>-1</sup>. The adsorption rate was primarily controlled by intra-particle diffusion, indicating that the pore size of the carbon was a significant factor. The results of XPS before and after Pb(II) adsorption revealed that the grafted amino groups enhanced the adsorption. The modified carbon was tested on real water samples and exhibited high removal capacities. These findings indicate that the bagasse MC could be a suitable precursor for the preparation of amino-rich mesoporous materials with significant Pb(II) adsorption performance.

*Keywords:* Bagasse; Mesoporous carbon; Microwave activation; Amino modification; Lead ion

### 1. Introduction

Environmental lead pollution is mainly caused by mining and battery casting, as well as residues of

paint, coatings, pesticides, chemical fertilizers, machines, tint, and glazes [1]. Lead can threaten human health by entering into and accumulating in organs through the skin, digestive tract, and respiratory tract. The toxic effects of lead include anemia, neurological

\*Corresponding authors.

<sup>1</sup>These authors contributed equally to the work.

disorder, and renal injury [2]. The permissible limits of lead in drinking and surface water intended for consumption are 0.010, 0.015, and 0.010 mg L<sup>-1</sup> as set by EU, USEPA, and WHO, respectively [3]. Therefore, reduction of lead to acceptable concentrations remains a challenge for treatments of drinking water and wastewater [4].

Traditional methods of lead removal from aqueous solutions include ion exchange, chemical reduction, use of separation membranes, electrochemical treatment, reverse osmosis, and distillation electrodialysis [5]. However, these methods often exhibit low efficiencies or require additional treatments [6]. In particular, lead removal is not ideal because of very low lead concentration. Therefore, a novel and cost-effective adsorbent for lead removal from aqueous solutions must be developed.

Porous carbons such as biochar, activated carbon (AC), mesoporous carbon (MC), carbon aerogel, and graphene are common adsorbents used to remove aqueous metals because these carbon materials exhibit excellent porous structures, specific surface properties, reusability, and minimal costs. However, porous carbons are more effective for adsorbing organic compounds than metal ions and inorganic pollutants because of the non-polar surface chemistry of these carbons. Therefore, several techniques, such as introducing other heteroatom-containing functional groups, have been utilized to modify the surface chemistry of porous carbon and enhance metal-removing capacity from aqueous solutions [6,7]. Numerous studies on the introduction of specific functional groups into porous carbon were conducted to improve adsorption toward specific adsorbates. For example, imidazole [8], thiol [9], and cetyltrimethylammonium bromide [10] have been used to modify porous material surfaces for chromium removal. According to Hard–Soft Acid–Base theory, lead ions interact strongly with nitrogen-containing ligands to form stable rings. Thus, adding nitrogen-containing groups on porous carbon could improve the adsorption of lead ions from aqueous solutions. The surface chemical modification of porous carbon is an effective approach for enhancing metal removal from aqueous media; however, some pores of the AC maybe blocked during the modification, thereby decreasing the adsorption efficiency for heavy metal ions [11].

Compared with traditional adsorbents, such as AC, MCs possess larger surface area, higher pore volume, adjustable pore structure, narrow pore size distribution, and unprecedented adsorption performance toward a wide range of inorganic and organic chemicals; MCs also exhibit fast adsorption kinetics, high adsorption capacity, and good stability. Specifically,

the MC surface can be easily modified to create specific binding sites for specific chemicals [12–14].

China is one of the largest producers of cane sugar and has the third largest plantation area worldwide; over 77.4 million metric tons of cane sugar are produced per production season [15]. As a consequence, sugarcane bagasse residues have become abundant, cheap, and readily available sources of lignocellulosic biomass in China. After sucrose extraction from sugar canes, the treatment and disposal of bagasse remains a challenge. Some studies have shown that bagasse-based adsorbents can efficiently remove heavy metals from wastewater [16–18]. Hence, bagasse could be used as a precursor for the production of amino-modified MCs with significant adsorption capacity for heavy metal ions. This innovation offers an opportunity to convert agricultural products to efficient adsorbents.

This study aims to demonstrate that bagasse is a suitable precursor for the preparation of amino-rich MC with significant adsorptive performance toward Pb(II) ions. In this study, we (1) prepared MC from bagasse, which features high surface area and mesoporosity, through microwave-assisted phosphate activation via an orthogonal experiment; (2) grafted amino groups on the prepared bagasse MC via nitric acid oxidation, followed by ethylenediamine polymerization; (3) studied the chemical bonding between amino groups and the modified carbon as well as mesoporous property through FTIR and X-ray photoelectron spectroscopy (XPS) analyses; (4) explored the role of mesopore structure and amino modification on Pb(II) adsorption through batch equilibrium experiments at different initial concentrations, pH values, temperatures, and contact times; and (5) investigated the interaction mechanisms between Pb(II) and bagasse MC via adsorption kinetics, thermodynamics, and XPS analyses.

## 2. Materials and methods

### 2.1. Preparation, modification, and characterization of MC

#### 2.1.1. Preparation of bagasse MC

Bagasse was produced in Zhejiang Province, China. An L<sub>9</sub> (3<sup>4</sup>) orthogonal design table was established to discuss the effects of impregnation ratio, drying time, activation power, and activation time on pore structure using methylene blue as probe. The results of methylene blue adsorption are shown in Table 1.

Bagasse was dried at 105°C for 48 h, ground, and then screened to particle sizes of 50–80 meshes. The powder was mixed with phosphoric acid at H<sub>3</sub>PO<sub>4</sub>/bagasse impregnation ratios of 1:1, 2:1, and 3:1

Table 1

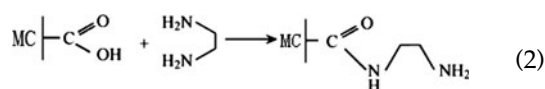
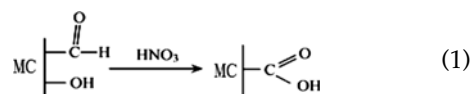
L<sub>9</sub> (3<sup>4</sup>) orthogonal array (levels of four different factors and obtained results for yield, methylene blue, and iodine value)

Samples	Impregnation ratio A (g:g)	Drying time B (/h)	Activation power C (w)	Activation time D (h)	Yield (%)	Methylene blue value (mg g <sup>-1</sup> )	Iodine value (mg g <sup>-1</sup> )	Surface area (m <sup>2</sup> g <sup>-1</sup> )
I1	1:1	6	700	10	42.09	204	819	–
I2	1:1	8	800	16	40.51	223	762	968
I3	1:1	10	900	22	39.20	229	817	1,021
I4	1:2	6	800	22	43.20	209	770	–
I5	1:2	8	900	10	43.36	220	726	–
I6	1:2	10	700	16	42.56	214	744	–
I7	1:3	6	900	16	41.54	223	737	816
I8	1:3	8	700	22	40.64	161	706	–
I9	1:3	10	800	10	42.33	183	721	–

for 24 h. The mixtures were pre-carbonized at 105 °C for 6–10 h and then activated in a microwave device for 10–22 min at 700–900 W power under nitrogen protection. The activated product was cooled to room temperature and washed with deionized water. The sample was poured into a beaker containing 0.1 mol dm<sup>-3</sup> HCl (250 cm<sup>3</sup>) and stirred for 2 h. Finally, the sample was washed with hot water until the pH of the washing solution reached 6–7. The dried powder was sieved in 0.18–0.42 mm mesh size, and the resulting sample was designated as bagasse-AC. Taguchi experimental design method was used to optimize the preparation conditions of bagasse MC, and the corresponding optimal values were evaluated using an L<sub>9</sub> (3<sup>4</sup>) orthogonal experiment. The variables and their levels are summarized in Table 1. The nine biomass carbon samples prepared via the L<sub>9</sub> (3<sup>4</sup>) orthogonal experiment under different conditions were named as I, I1, I2, and so on.

### 2.1.2. Modification of bagasse MC

The prepared MC I7 was modified. About 5 g of the purified MC I7 was poured into 300 mL of 32.5% nitric acid and reacted at 60 °C for 5 h. The oxidation sample MC-HNO<sub>3</sub> was mixed with 125 mL of ethylenediamine and 5 g of dicyclohexylcarbodiimide and then reacted at 120 °C for 24 h. The obtained product was successively washed with ethyl alcohol and ethylether. After drying at 105 °C, amino-modified MC I7-EDA was produced. The reaction mechanism of the modification was:



### 2.1.3. Characterization of bagasse

The pore structure of the samples was determined using a Micromeritics ASAP2020 volumetric adsorption apparatus with high purity N<sub>2</sub> as the absorbing medium at -196 °C. The relative pressure ( $P/P_0$ ) was within the range of 10<sup>-6</sup>–0.98. The total surface area of the MC was determined using the BET method, whereas the volumes of micropores and mesopores were calculated according to the *t*-plot and BJH equations, respectively. Pore size distribution was characterized using the DFT equation. Bruker Tensor 27 type Fourier transform infrared spectrometer was used to determine the identity of surface functional groups. PHI 5,000 Versa Probe X-ray electron spectrometer from Ulvac-Phi was used to acquire the XPS images of the carbons before and after Pb(II) absorption.

## 2.2. Adsorption experiments

### 2.2.1. Adsorption isotherm

A specific amount (0.1000 g) of the sample was placed to 250 mL triangular flasks containing 100 mL of Pb(NO<sub>3</sub>)<sub>2</sub> solutions with 30–200 mg L<sup>-1</sup> Pb(II) at pH4.5. No pH adjustment was performed in the sorption process. The flasks were placed in an air bath constant-temperature shaker and vibrated at 25 °C, 35 °C, and 45 °C for 24 h. After sorption, the adsorbents were separated by filtration through a 0.45 μm membrane. The residual Pb(II) concentrations in the filtrate were analyzed with an inductively coupled plasma optical emission spectrometry (IRIS Interpid II XSP).

All experiments were performed in duplicate. The removal rate ( $R$ , %) and adsorption amount of Pb(II) per unit mass of the adsorbent at equilibrium ( $q_e$ ,  $\text{mg g}^{-1}$ ) were calculated using the following equations:

$$q_e = V(c_0 - c_e)/m \quad (3)$$

$$R(\%) = (c_0 - c_e)/c_0 \times 100 \quad (4)$$

where  $c_0$  and  $c_e$  are the initial and equilibrium concentrations ( $\text{mg L}^{-1}$ ) of the adsorbent in the solution, respectively;  $V$  is the volume of the solution; and  $m$  is the mass of the adsorbent (g).

### 2.2.2. Influence of pH

In experiments on the effect of pH, the initial pH values of the solution were within the range of 2.0–8.0 and regulated by adding  $0.01 \text{ mol}\cdot\text{L}^{-1}$  NaOH and  $\text{HNO}_3$ . The adsorbent (0.1000 g) was placed in a 250 mL flask containing 100 mL of  $\text{Pb}(\text{NO}_3)_2$  solution with  $150 \text{ mg}\cdot\text{L}^{-1}$  Pb(II). The flask was vibrated at  $25^\circ\text{C}$  and  $150 \text{ r min}^{-1}$  for 24 h until the adsorption equilibrium was achieved.

### 2.2.3. Kinetics of adsorption

Kinetics experiments were conducted in a covered 500 mL conical flask to prevent water evaporation. Then, 250 mL of  $100 \text{ mg L}^{-1}$  or  $150 \text{ mg L}^{-1}$  Pb(II) solution was placed in the flask, and the pH was adjusted to 4.5. The flask was placed in a DF-II thermal magnetic stirrer to control the experimental temperature. Timing began once 0.2500 g of the adsorbent was added to the solution. In the first 10 min, samples

were obtained every 2 min and every 30 min thereafter.

### 2.3. Desorption and reusability studies

The adsorbent was first saturated with Pb(II) by placing  $1.0 \text{ g L}^{-1}$  adsorbent in 100 mL of  $200 \text{ mg L}^{-1}$  Pb(II) solution to evaluate regeneration capacity. The mixture was stirred for 24 h at  $45^\circ\text{C}$ , as described in Section 2.2. After equilibration, the adsorbent was dried at  $60^\circ\text{C}$  for 12 h and then dispersed in 1 M  $\text{HNO}_3$ . The Pb(II)-loaded adsorbent was subjected to ultrasound treatment and filtration, and the amount of desorbed  $\text{Pb}^{2+}$  was measured. After regeneration, the adsorbent was rinsed with DI water and used in subsequent adsorption experiments. The adsorption–desorption process was investigated in five time cycles.

## 3. Results and discussion

### 3.1. Characterization of synthesized samples

#### 3.1.1. Methylene blue value, BET surface area, and pore volume

In accordance with the classification system adopted by the International Union of Pure and Applied Chemistry (IUPAC) [19], adsorbent pores are classified into three groups: micropores (size  $<2 \text{ nm}$ ), mesopores ( $2\text{--}50 \text{ nm}$ ), and macropores ( $>50 \text{ nm}$ ). The most common standard parameters for measuring carbon adsorptive capacity are iodine value, molasses number, and methylene blue value, which define the micropores, mesopores, and macropores, respectively [20]. The effect of impregnation ratio, drying time, activation power, and activation time on the pore structure of  $\text{H}_3\text{PO}_4$ -activated bagasse carbon was

Table 2  
Range and ANOVA analysis of methylene blue value

Parameters	Impregnation ratio A (g:g)	Drying time B (h)	Activation power C (w)	Activation time D (h)
Range analysis				
K1	218.67	212.00	193.00	202.33
K2	214.33	201.33	205.00	220.00
K3	189.00	208.67	224.00	199.67
R	29.67	10.67	31.00	20.33
ANOVA analysis				
Sum of squares	770.34	89.34	733.00	366.34
F-ratio	8.62		8.21	4.10
Percent (%)	39	5	37	19

evaluated by microwave treatment, and an  $L_9$  ( $3^4$ ) orthogonal design table was established (Table 1).

ANOVA was used to determine the degree of variation of each factor relative to the total variation in the result. Table 2 shows that activation power exhibited the largest variance, followed by impregnation ratio. The most significant factor affecting methylene blue value was activation power, followed by impregnation ratio, activation time, and drying time. Methylene blue is mainly adsorbed in mesopores and is therefore used to indicate the mesopore number of the AC [20,21]. Among the prepared carbon samples, I2, I3, and I7 showed the highest adsorption of methylene blue, indicating their high mesoporosity.

The surface area and pore structure of carbon samples I2, I3, and I7 were further investigated by  $N_2$  sorption measurements. As shown in Fig. 1, the amount of  $N_2$  adsorption of I2, I3, and I7 increased greatly at low relative pressures ( $P/P_0 \leq 0.01$ ), indicating the presence of micropores [5]. A hysteresis loop was observed instead of overlapping nitrogen adsorption for carbon samples I2 and I3 at  $P/P_0 = 0.4$ . An adsorption platform appeared, but no drift was observed at the end. These findings conform to the IV isotherm characteristics provided by IUPAC classification. These results indicate that pore structures of I2 and I3 are mainly composed of micropores and mesopores. Similarly, a hysteresis loop was observed on the nitrogen adsorption–desorption isotherms of I7 at  $P/P_0 = 0.4$ , indicating that I7 also contains numerous mesopores. Further calculation showed that the BET-specific surface areas of I2, I3, and I7 are 968, 1,021, and 816  $m^2 g^{-1}$ , respectively; and their total pore volumes are 0.669, 0.647, and

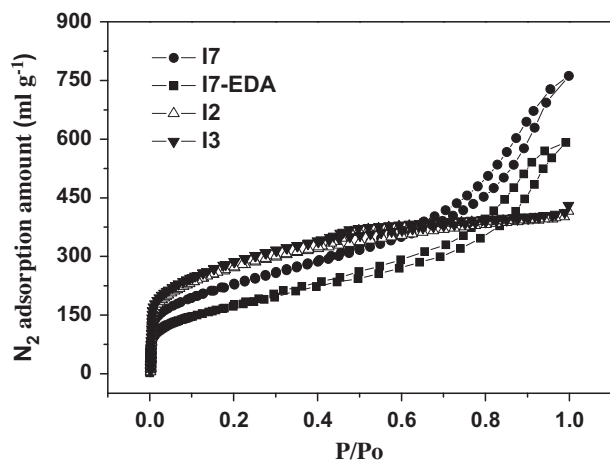


Fig. 1. Nitrogen adsorption–desorption isotherms of bagasse-ACs before and after modification.

1.184  $cm^3 g^{-1}$ , respectively. The proportions of mesopores for I2, I3, and I7 reached as high as 47.8, 51.2, and 91.9%, respectively. These findings confirm that the prepared I2, I3, and I7 are made of MC; as such, carbon I7, having the highest mesopore volume, was used to graft amino groups for efficient adsorption removal of Pb(II). The nitrogen adsorption–desorption isotherms of modified I7 (I7-EDA) are shown in Fig. 1. Compared with that of the pristine I7, the BET specific surface area, total pore volume, and mesoporosity of I7-EDA decreased to 721  $m^2 g^{-1}$ , 0.784  $cm^3 g^{-1}$ , and 73%, respectively. Data showed that the carbon I7-EDA belongs to typical MC, although parts of the carbon's pores were blocked during modification.

### 3.1.2. FT-IR analysis

The FTIR spectra of I7 and I7-EDA are shown in Fig. 2. Adsorption peaks on I7 were observed at 496, 670, 1,169, 1,580, and 1,692  $cm^{-1}$ . The major peak at 1,169  $cm^{-1}$  is due to the stretching and bending vibrations of the  $\gamma_{C-C}$  framework containing ketone, whereas the major peak at 1,580  $cm^{-1}$  is induced by the  $\gamma_{C=O}$  stretching vibration of  $\beta$ -ketone. The adsorption peak at around 1,693  $cm^{-1}$  is attributed to the  $\gamma_{C=O}$  stretching vibration of  $\alpha,\beta$ -unsaturated aldehyde [22,23]. The modification led to the formation of new functional groups. In the FTIR spectra of the modified I7-EDA, new peaks appeared at 405, 1,061, 1,212, 1,382, and 1,531  $cm^{-1}$ ; and the bands attributed to amino groups were strongly enhanced. The characteristic peaks at 1,531 and 1,212  $cm^{-1}$  are attributed to the bending of  $\gamma_{N-H}$  and the stretching of C–N in fatty

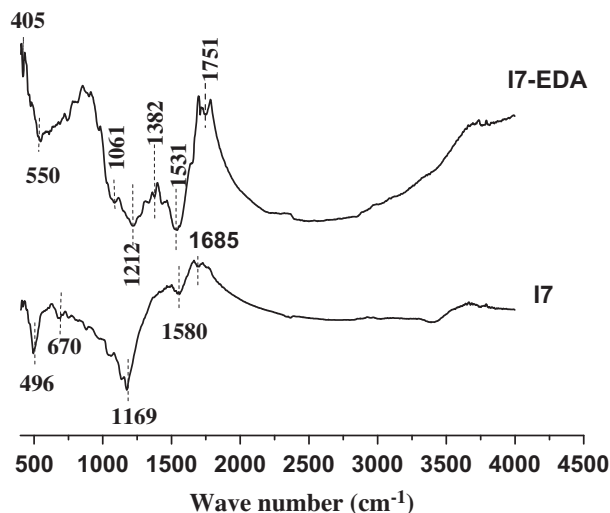


Fig. 2. FT-IR spectra of bagasse-AC I7 before and after modification.

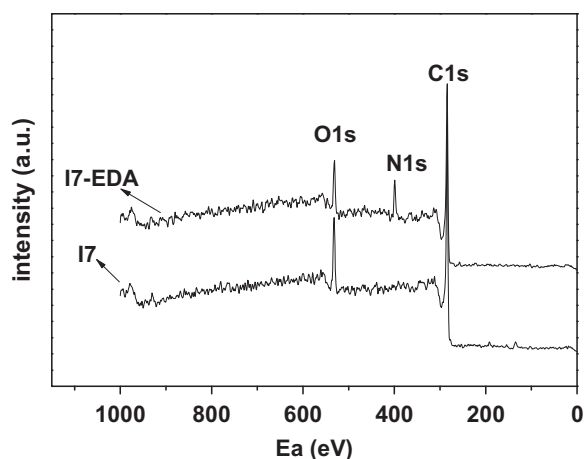


Fig. 3. XPS spectra of bagasse-AC I7 before and after modification.

amine or aromatic secondary amine [24,25]. The adsorption peak at  $1,382\text{ cm}^{-1}$  is attributed to the stretching vibration of  $\gamma_{\text{-N=C=O}}$ , whereas the adsorption peak at  $1,061\text{ cm}^{-1}$  is produced by the stretching vibration of  $\gamma_{\text{-C-O-C}}$  [26,27]. These new peaks resulting from nitrogen-containing functional groups appeared on I7-EDA, thereby indicating that amino groups were successfully introduced after the modification.

### 3.1.3. XPS analysis

The surface chemical properties of bagasse MC I7 before and after modification were investigated via XPS (Fig. 3). The full score revealed that C 1s and O 1s peaks appeared successively in the prepared carbon I7, whereas the N 1s peak appeared in the I7-EDA sample at the location with a binding energy of

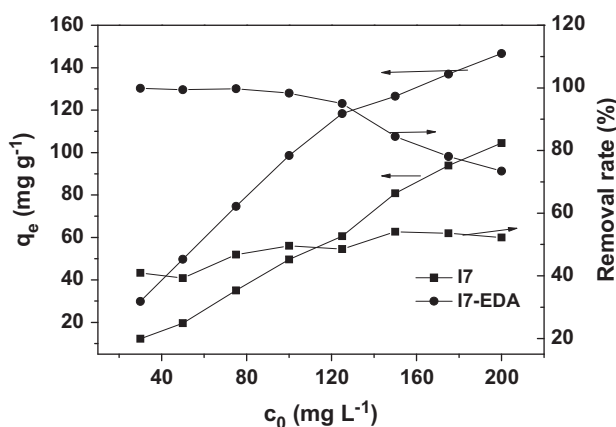


Fig. 4. Influence of modification of Pb(II) adsorption on I7 at different concentrations.

400 eV. The result further implies that amino groups were successfully grafted on I7-EDA after the modification [28,29].

### 3.2. Influence of modification

Pb(II) adsorption by I7 and I7-EDA at different concentrations at  $25^\circ\text{C}$  is displayed in Fig. 4. A significant difference in Pb(II) adsorption capacity and removal rate was observed between the pristine I7 and modified I7-EDA. When Pb(II) concentration was less than  $60\text{ mg L}^{-1}$ , almost all of the Pb(II) was absorbed by I7-EDA; only 45% of Pb(II) was eliminated by the pristine I7. Both Pb(II) adsorption capacities of I7 and I7-EDA significantly increased with increasing initial Pb(II) concentration. At Pb(II) concentrations  $>200\text{ mg}\cdot\text{L}^{-1}$ , the maximum Pb(II) adsorption capacity of I7-EDA is  $150\text{ mg g}^{-1}$ , which is about 1.5 times higher than that of I7. I7-EDA maintained a high removal rate for Pb(II) with increasing Pb(II) concentration, and the removal rate was higher than 85% even when the Pb(II) concentration reached  $150\text{ mg L}^{-1}$ . However, the removal rate of Pb(II) by I7 was less than 50%. The adsorption of metal ions by functional porous materials was determined by their diffusibility and surface chemical properties (e.g. complexing power, steric effect, and hydrophilicity of the functional materials) [30,31]. Generally, chemical modification decreases pore volume and specific surface area of materials. However, in the present experiment, I7-EDA exhibited higher Pb(II) adsorption capacity than I7, showing that I7-EDA is superior in eliminating Pb(II) from aqueous solutions than I7. This finding reflects that the Pb(II) adsorption capacity of MC can be greatly enhanced through amination modification.

### 3.3. Influence of pH

The effect of pH of the solution is an important parameter that controls the adsorption process. pH controls the surface charge of adsorbents, the degree of ionization, and the speciation of adsorbate species. Depending on pH, Pb(II) potentially exists as  $\text{Pb}^{2+}$ ,  $\text{Pb}(\text{OH})^+$ ,  $\text{Pb}(\text{OH})_2$ ,  $\text{Pb}(\text{OH})_3^-$ ,  $\text{Pb}(\text{OH})_4^{2-}$ ,  $\text{Pb}_2(\text{OH})_3^-$ , and  $\text{Pb}_3(\text{OH})_4^{2-}$  in aqueous solutions [32,33]. Pb(II) predominantly appeared in the cationic form ( $\text{Pb}^{2+}$ ) at  $\text{pH} < 6$  [33] and was hydrolyzed to  $\text{Pb}(\text{OH})^+$  between  $\text{pH} 6$  and  $8$ . Solid  $\text{Pb}(\text{OH})_2$  was found to be the most thermodynamically stable phase at  $\text{pH} > 9.0$ , whereas  $\text{Pb}(\text{OH})_3^-$  was predominant at  $\text{pH}$  above  $11$  [34]. Therefore, a range of pH values between  $2$  and  $8$  was further tested.

As shown in Fig. 5, the influence of solution pH on the adsorption of Pb(II) on I7-EDA was

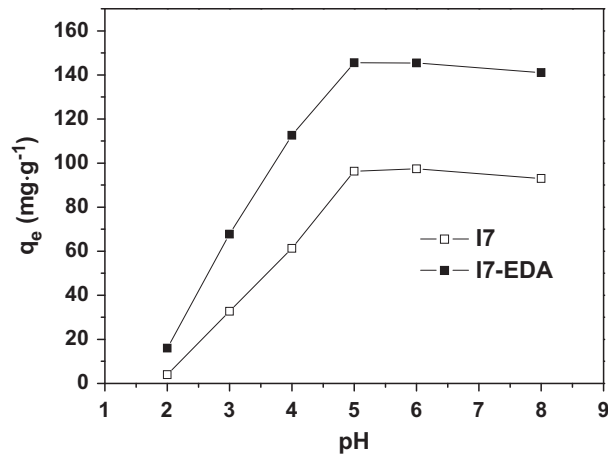


Fig. 5. Influence of solution pH on the adsorption of Pb(II) on I7 and I7-EDA.

investigated with an initial pH range of 2.0–8.0 at 25°C. For comparison, the adsorption by I7 was also conducted at the same pH range. In the measured range of pH, I7-EDA showed larger Pb(II) adsorption capacity than I7, showing that the modification improved the Pb(II) adsorption properties of I7. Moreover, Fig. 5 shows that the sorption of Pb(II) increased quickly at pH < 4, stabilized at pH 5–6, and decreased slightly at pH > 6. pH is one of the most important parameters affecting the adsorption process of metal ions.

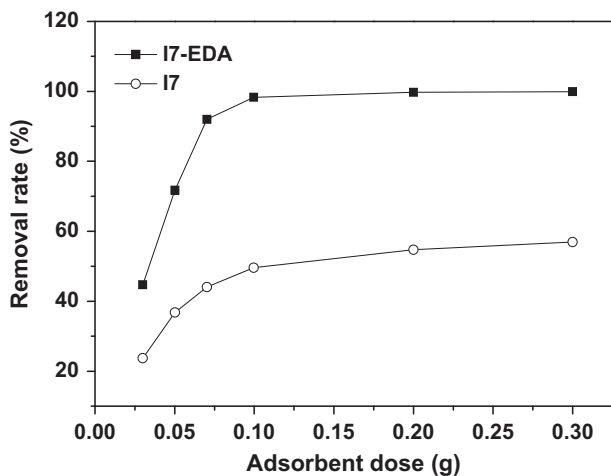
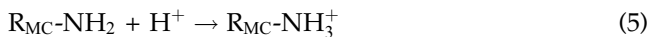
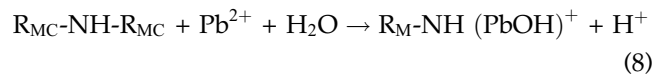
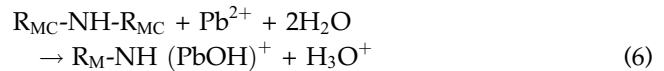


Fig. 6. Effect of adsorbent dose on the removal efficiency of Pb(II) on I7 and I7-EDA.



In these reactions,  $R$  represents the modified MC matrix. Based on the results of the acid/base titration, the point of zero charge (pzc) value of the modified I7 was about 4.9. At pH < pHPzc, the surface charge of the modified I7 was positive because the amino groups easily combined with  $H^+$  in acidic media where protonation occurs [35,36] Eq. (5). Obviously, lower solution pH can result in more positively charged amino groups, which is unfavorable for coordination of Pb ions by the modified I7 Eqs. ((6)–(8)) because of electrostatic repulsion. However, the surface charge of the modified I7 at pH > pHPzc was negative because of the adsorption of  $OH^-$  ions through hydrogen bonding at high pH values Eq. (9). The slow decrease in Pb(II) removal at pH > 6.0 was attributed to the precipitation reaction of Pb(II). pH 4.5 was chosen for further studies to avoid the hydrolysis of Pb(II) ions at higher pH values and simultaneously identify the elements.

### 3.4. Effect of adsorbent dosage

Batch experiments were conducted to determine the effect of adsorbent dosage on Pb(II) removal by I7 and I7-EDA under similar conditions (initial concentration of 100 mg L<sup>-1</sup>, pH 4.5, sorption time of 24 h at 25°C, as shown in Fig. 6). The experimental results revealed that the removal efficiencies of Pb(II) increased gradually with increasing amounts of the two adsorbents. Increasing the mass of I7 from 0.010 to 0.300 g significantly enhanced the removal percentage of Pb(II) from 23.7 to 56.9% for I7 and from 44.75 to 99.9% for I7-EDA (Fig. 6). The increase in adsorption with dosage can be attributed to the increased availability of active adsorption sites for metal ion binding. The high removal of Pb(II) by I7-EDA was caused by the synergy of amino and carboxyl functionality. The removal rate of Pb<sup>2+</sup> increased to 98.3% with the increase in the adsorbent dose to 0.10 g/100 mL and reached its maximum (99.7%) at about 0.20 g/100 mL. This finding suggests that the

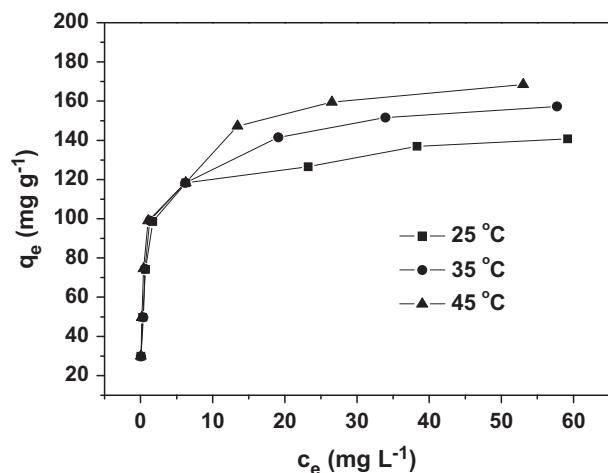


Fig. 7. Adsorption isotherms of Pb(II) on I7-EDA at 25°C, 35°C, and 45°C.

economic absorbent dose for the removal of  $\text{Pb}^{2+}$  in this system is 0.10 g/100 mL.

### 3.5. Influence of temperature

The Pb(II) adsorption isotherms of I7-EDA at 25, 35, and 45°C are shown in Fig. 7. The influence of temperature on Pb(II) adsorption of I7-EDA varied with the initial Pb(II) concentration. When Pb(II) concentration was lower than 10 mg L<sup>-1</sup>, the Pb(II) adsorption by I7-EDA was slightly influenced by solution temperature. However, the effect of temperature intensified gradually with increasing Pb(II) concentration. Given

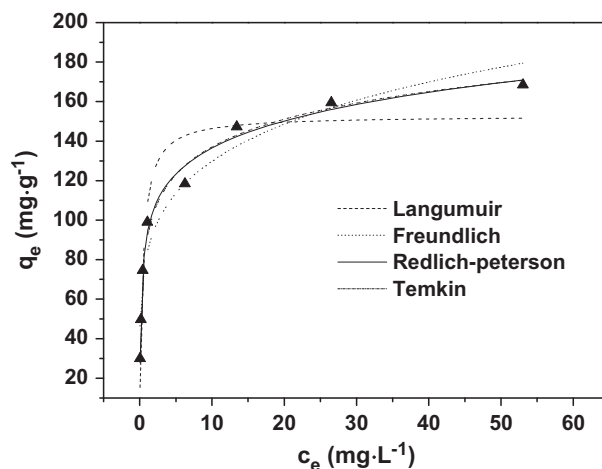


Fig. 8. Comparison of fitting curves of Pb(II) adsorption isotherm on I7-EDA via different models.

the same initial Pb(II) concentration of 200 mg L<sup>-1</sup>, the equilibrium concentrations of Pb(II) after adsorption by I7-EDA at 25, 35, and 45°C are 48, 42, and 35 mg L<sup>-1</sup>, respectively. The corresponding equilibrium adsorption capacities ( $q_{\text{mea}}^0$ ) are 151, 172, and 185 mg g<sup>-1</sup>, respectively, showing that high temperatures enhance Pb(II) adsorption. This finding implies that Pb(II) adsorption by I7-EDA is an endothermic reaction, and chemical reaction dominates the adsorption process.

The Langmuir, Freundlich, Redlich–Peterson, and Temkin isotherm models were applied to analyze the adsorption characteristics of Pb(II) on I7-EDA. The fitting curves of Pb(II) adsorption isotherms via different

Table 3  
Isotherm parameters of Pb(II) on I7-EDA at different temperatures

Isotherms	Parameters	Temperature (°C)		
		25°C	35°C	45°C
Langmuir $q_e = bq^0c_e/(1 + bc_e)$	$q_{\text{cal}}^0$ (mg g <sup>-1</sup> )	134	149	153
	$q_{\text{mea}}^0$ (mg g <sup>-1</sup> )	151	172	185
	$b$ (L·mg <sup>-1</sup> )	1.94	1.48	2.25
	$R^2$	0.945	0.938	0.917
Freundlich $q_e = K_{\text{FCe}}^{1/n}$	$K_{\text{F}}$ (L·mg <sup>-1</sup> )	76	78	83
	$n$	6.04	5.31	5.16
	$R^2$	0.910	0.932	0.949
Redlich-Peterson $q_e = K_{\text{RCe}}/(1 + ac_e^\beta)$	$K_{\text{F}}$ (L·mg <sup>-1</sup> )	576	566	918
	$A$ (L·mg <sup>-1</sup> )	5.79	5.66	8.89
	$\beta$	0.912	0.883	0.872
	$R^2$	0.968	0.962	0.986
Temkin $q_e = B \ln A_{\text{T}} + B \ln c_e$	$A_{\text{T}}$ (L·mg <sup>-1</sup> )	155	86	88
	$B$ (L·mg <sup>-1</sup> )	15.9	19	20
	$R^2$	0.968	0.969	0.988

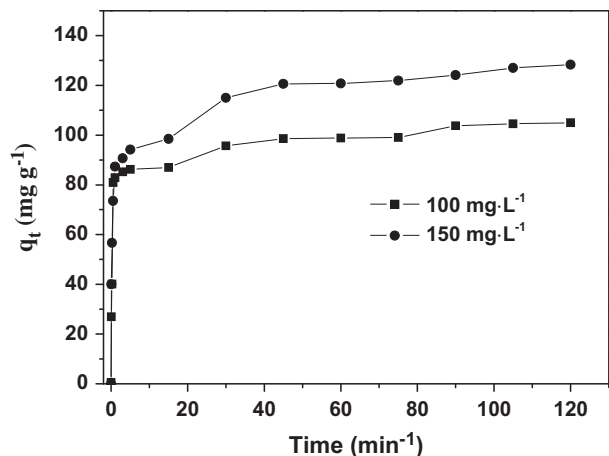


Fig. 9. Effect of contact time on Pb(II) adsorption on I7-EDA.

models at 45°C are shown in Fig. 8. The nonlinear fitting parameter results are listed in Table 3. Fig. 8 shows that the Redlich–Peterson and Temkin fitting curves agree with experimental data, but the Langmuir fitting curve shows poor degree of fitting with experimental data. Furthermore, the correlation coefficient ( $R^2$ ) of both Redlich–Peterson and Temkin fitting curves are higher than those of Langmuir and Freundlich fitting curves. In addition, the calculated maximum adsorption amount ( $q_{cal}^0$ ) was far away from the measured adsorption amount ( $q_{mea}^0$ ). These results indicate that Redlich–Peterson and Temkin models described Pb(II) adsorption on I7-EDA better, whereas the Langmuir model was inappropriate to depict the adsorption. This finding indicates that the energy distribution on the I7-EDA surface is inhomogeneous. Some I7-EDA surface sites have higher energies and affinity, whereas others have lower energies and weak affinity [37–40]. This finding also implies that Pb(II) adsorption by I7-EDA belongs to multilayer adsorptions, including surface physical adsorption and monolayer internal chemical adsorption. The Freundlich constants of  $n$  were found to be more than 1 for all temperatures, which indicates that the adsorption is favorable.

### 3.6. Adsorption kinetics

The influence of time on the adsorption of Pb(II) by I7-EDA is shown in Fig. 9. At different Pb(II) concentrations, the kinetic adsorption of Pb(II) by I7-EDA exhibited similar characteristics. In the early period, the adsorption capacity increased rapidly and reached over 70% of the total adsorption within 5 min. The

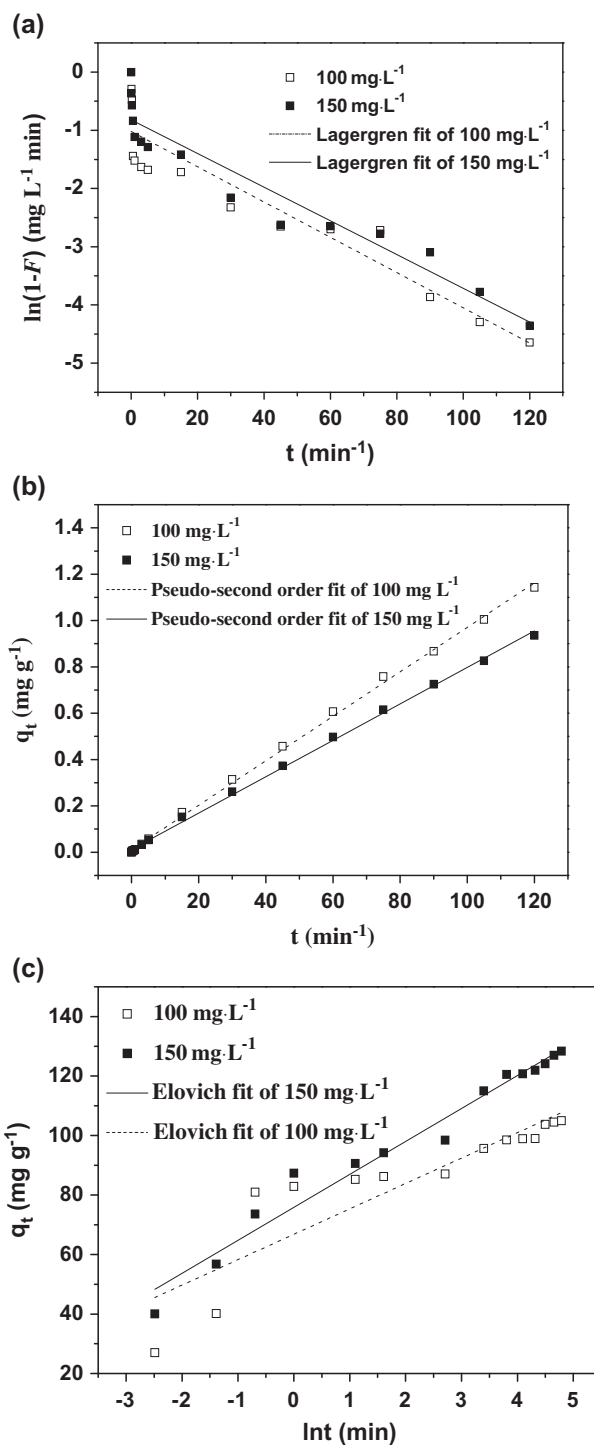


Fig. 10. Linear fitting curves of adsorption kinetics of Pb(II) on I7-EDA, (a) Lagergren first-order model, (b) pseudo-second-order model, and (c) Elovich model.

adsorption amount  $q_t$  slowly increased until the peak appeared 30 min later and the equilibrium was observed. The high efficiency of adsorption should be

Table 4  
Parameters of three kinetic models for Pb(II) adsorption by I7-EDA

Kinetic model	Parameters	100 mg·L <sup>-1</sup>	150 mg·L <sup>-1</sup>
Lagergren $\ln(1 - q_t/q_e) = -k_1 t$	$k_1$ (min <sup>-1</sup> )	1.021	0.820
	$R^2$	0.863	0.914
Pseudo-second-order $t/q_t = 1/k_2 q_e^2 + t/q_e$	$q_{e,mea}$ (mg g <sup>-1</sup> )	106	130
	$q_{e,cal}$ (mg g <sup>-1</sup> )	104	127
	$k_2$ (g (mg min) <sup>-1</sup> )	0.00959	0.00786
	$R^2$	0.9987	0.9986
	$q_{e,mea}$ (mg g <sup>-1</sup> )	106	130
Elovich $q_t = (1/\beta_E) \ln(\alpha_E \beta_E) + (1/\beta_E) \ln t$	$\alpha_E$ (mg (g min) <sup>-1</sup> )	21,294	10,465
	$\beta_E$ (g mg <sup>-1</sup> )	0.117	0.0903
	$R^2$	0.791	0.966
	$q_{e,mea}$ (mg g <sup>-1</sup> )	106	130

related to the large amount of active amino groups, such as -NH<sub>2</sub>, on the surface of I7-EDA. In addition, the active-NH<sub>2</sub> groups were mainly located on the middle and outer surfaces of the I7-EDA mesopores. Thus, the mass transfer resistance is low, thereby facilitating the adsorption of ions into the adsorption site.

The Lagergren first-order and pseudo-second-order models as well as the Elovich model were adopted to analyze the kinetic process of Pb(II) on the mesoporous I7-EDA (Fig. 10). The parameters fitted from the kinetic equations are shown in Table 4. Based on the correlation coefficients ( $R^2$ ) obtained, the pseudo-second-order model best fitted the adsorption kinetics of Pb(II) on the mesoporous I7-EDA at two different concentrations. In addition, the theoretical equilibrium adsorption capacity  $q_e$  were approximate to the capacity measured from the experiments. This analysis reveals that the pseudo-second-order kinetics equation describes the adsorption behavior well and is consistent with the kinetic mechanism of adsorbing heavy metal ions by other adsorbents [41,42]. Chemical adsorption could be inferred to dominate the adsorption process because the formation of chemical bond is the main factor that influences the pseudo-second-order adsorption [43]. This result is in accordance with the mechanism of reaction between the functional group of I7-EDA and Pb(II) ions. The second-order kinetic model covered the whole adsorption process, thereby reflecting a real and complete kinetic mechanism of Pb(II) ion adsorption.

### 3.7. Adsorption mechanism

#### 3.7.1. Adsorption rate controlling steps

Three steps in the adsorption and removal of heavy metal ions on porous materials include the diffusion of heavy metal ions from the solution to the surface of the porous material through a liquid film, diffusion from

the surface to the inside of a porous material, and the chemical reaction of ions on the active group of the porous material. The adsorption by porous materials is affected by the speed of the three steps, with controlling the adsorption rate as the slowest step. Generally, the last step is the fastest; the adsorption equilibrium can be established rapidly on each site on the surface of micropores. Thus, the total adsorption rate is controlled by film diffusion, pore diffusion, or both. The equation of the Weber–Morris intra-particle diffusion model was used to analyze the kinetics data of Pb(II) adsorption by I7-EDA to determine the steps of controlling the adsorption rate. The Weber–Morris intra-particle diffusion equation [44] is:

$$q_t = K_w t^{0.5} + b \quad (10)$$

where  $K_w$  is the inner diffusion rate constant [mg·(g·min<sup>0.5</sup>)<sup>-1</sup>],  $t$  is the adsorption time, and  $b$  reflects the boundary layer effect. The figure was drawn according to  $q_t$  and  $t^{0.5}$ , and the slope of the straight line is  $K_w$ . Weber and Morris thought that if  $q_t$  and  $t^{0.5}$  have a linear relation that passes the origin, the adsorption is controlled by intra-particle diffusion; however, if the line does not pass the origin, a larger  $b$  indicates that film diffusion greatly influences adsorption rate [45,46].

Fig. 11 shows the Weber–Morris adsorption curve of Pb(II) adsorption on I7-EDA at two different concentrations. The fitting parameters are shown in Table 5. The adsorption of Pb(II) on I7-EDA resulted from the joint effect of the physical adsorption and chemical action between amino groups and Pb(II) ions. In general,  $q_t$  to  $t^{0.5}$  displays many segments, implying that the adsorption rate is controlled by inner and film diffusions. Cluster analysis shows that the Webber–Morris curve of the adsorption is divided into two linear stages. That is, the straight line near

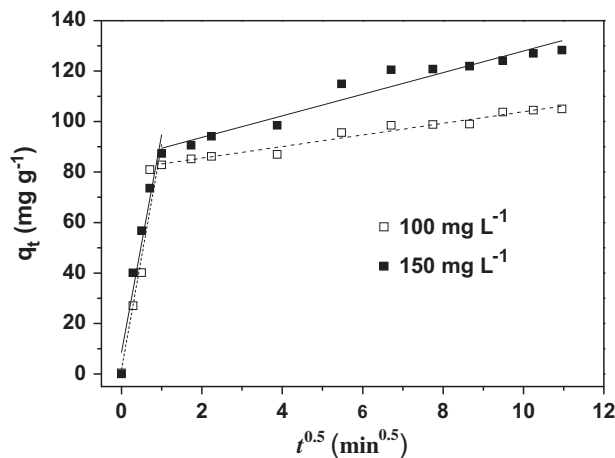


Fig. 11. Intra-particle diffusion equation plots for Pb(II) adsorption on I7-EDA.

the origin indicates that within this period of time, the adsorption rate was faster and mainly controlled by the intra-particle diffusion; whereas the other one does not pass the origin and the intercept  $b$  is quite large, indicating that film diffusion was the dominant step that controlled the adsorption rate at this period of time. As shown in Table 5, the  $R^2$  values fitted from the Webber–Morris model are all higher than 0.9, indicating that this model can explain the adsorption process. The result  $k_{w1} > k_{w2}$  is in line with the previous analysis, which states that the adsorption rate at the early period was faster and slowed down afterwards. The  $R^2$  in the intra-particle diffusion model is smaller than that in the second-order kinetics model because of two reasons. Compared with the number of ions in the solution, the lead ions removed from the solution can be neglected. In addition, the intra-particle diffu-

sion strongly depended on the concentration of the solid phase in the adsorption system.

### 3.7.2. Adsorption energy

The isothermal adsorption data were fitted through the Dubinin–Kaganer–Radushkevick (D–K–R) model, and the adsorption heat of Pb(II) on I7-EDA was calculated. The D–K–R equation is given by [47]:

$$\ln q_e = \ln q_m - \beta \varepsilon^2 \quad (11)$$

where  $q_e$  is the equilibrium adsorption capacity ( $\text{mol}\cdot\text{g}^{-1}$ ),  $q_m$  is the adsorption capacity on each monomolecular layer ( $\text{mol}\cdot\text{g}^{-1}$ ),  $\beta$  is the relative constant of the adsorption energy ( $\text{mol}^2\cdot\text{J}^{-2}$ ), and  $\varepsilon$  is the Polanyi adsorption potential energy given by:

$$\varepsilon = RT \ln(1/c_e) \quad (12)$$

where  $R$  is the gas constant ( $8.314 \text{ J}\cdot(\text{mol}\cdot\text{K})^{-1}$ ),  $T$  is the absolute temperature (K), and  $c_e$  is the equilibrium adsorption concentration  $\text{mol}\cdot\text{g}^{-1}$ . According to  $\ln q_e$  and  $\varepsilon^2$ , the slope is the value, and the adsorption capacity can be derived according to the intercept. The Hobson formula is given by [48]:

$$E = -1/\sqrt{-2\beta} \quad (13)$$

where  $\beta$  and  $E$  meet the relational expression and  $E$  is the adsorption energy,  $\text{kJ}\cdot\text{mol}^{-1}$ .

The fitting results of the isothermal data of Pb(II) adsorption on I7-EDA at 25, 35, and 45°C through the D–K–R equation are shown in Table 6. The maximum

Table 5  
Results from linear regression of intraparticle diffusion equation plots

$c_0$ ( $\text{mg g}^{-1}$ )	$K_{1w}$ ( $\text{mg g}^{-1} \text{ min}^{-0.5}$ )	Equation	$R_1^2$	$K_{2w}$ ( $\text{mg g}^{-1} \text{ min}^{-0.5}$ )	Equation	$R^2$
100	81.51	$q_t = 89.29 t^{0.5} + 1.708$	0.9032	2.298	$q_t = 2.298 t^{0.5} + 80.92$	0.9628
150	86.16	$q_t = 86.16 t^{0.5} + 8.544$	0.9375	4.281	$q_t = 4.281 t^{0.5} + 85.15$	0.9408

Table 6  
DKR isotherm parameters of Pb(II) adsorption on I7-EDA

Temperature ( $^{\circ}\text{C}$ )	$q_m$ ( $\text{mg g}^{-1}$ )	$E$ ( $\text{kJ mol}^{-1}$ )	$\beta$ ( $\text{mol}^2 \text{ J}^{-2}$ )	$R^2$
45	178	11.98	3.54E-09	0.972
35	163	11.97	3.49E-09	0.973
25	150	12.52	3.19E-09	0.982

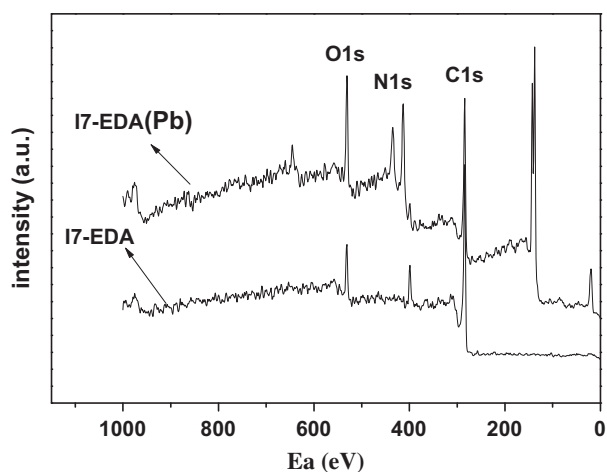


Fig. 12. XPS of I7-EDA before and after Pb(II) adsorption.

adsorption capacity increased with increasing temperature, implying that the adsorption is an endothermic reaction controlled by temperature. Adsorption energy within 1–8 and 9–16  $\text{kJ mol}^{-1}$  corresponds to physical and chemical adsorption, respectively [49]. Table 6 shows that the adsorption energy in the adsorption of Pb(II) on I7-EDA at 25, 35, and 45°C is higher than 11  $\text{kJ mol}^{-1}$ , thereby implying that the adsorption process is a chemical reaction.

### 3.7.3. XPS spectra

Various interactions between metal ions and the carbon surface is possible, such as formation of surface complexes, ion-exchange processes with the participation of strong surface acidic groups, and redox reactions with changes in metal valence [50,51]. XPS analysis was performed for sorbents prior to and after Pb(II) adsorption to investigate the interactions between lead ions and carbon surface. Fig. 12 shows that the spectrum of I7-EDA after Pb(II) adsorption

displayed new signals on the locations where the binding energies are 138, 436, and 641 eV. The results further demonstrate that the adsorption of Pb(II) was carried out by chemisorption. Moreover, the N1s peak displayed an evident left shift after the adsorption, which implies that a chemical reaction occurred between I7-EDA and Pb(II). The nitrogen atoms of the amino groups on the modified carbon I7-EDA contain free pairs of electrons that can potentially bind to Pb(II) ions or  $\text{H}^+$  ions, forming a coordination complex through electron pair sharing Eqs. ((6)–(8)). The combination of more negatively charged surfaces and the presence of amino groups induced by the modification could be responsible for the enhanced Pb(II) ion adsorption by I7-EDA. Notably, besides ion exchange, the physical adsorption in microspores and mesopores of modified carbons has an important role in the adsorption of lead species because the pristine carbon I7 with few amino groups exhibits a high adsorption capacity for Pb(II).

### 3.8. Regeneration

The regeneration of adsorbents is essential in reducing the overall cost of its application. As described in Section 3.3, the I7-EDA surface is protonated by  $\text{H}_3\text{O}^+$  ions under acidic conditions to facilitate Pb(II) desorption. The competition of  $\text{H}^+$  ions in the adsorption sites promotes the release of the adsorbed Pb(II)<sup>+</sup> into the aqueous solution, indicating that acid treatment may be a feasible approach for regeneration. Regeneration and adsorption by 1.0 mol  $\text{L}^{-1}$   $\text{HNO}_3$  were repeated five times. Preliminary results showed that during regeneration, the adsorption capacity of Pb(II) are 169.7, 167.3, 161.2, 157.2, and 156.3  $\text{mg g}^{-1}$  for the first, second, third, fourth, and fifth reuse cycles, respectively. The results show that I7-EDA could be reused for at least five times with –7.89% regeneration loss in its initial adsorption capacity. The regeneration and reuse performance of

Table 7  
Comparison of maximum adsorption capacities ( $q_{\text{max}}$ ) of  $\text{Pb}^{2+}$

Sorbents	Modified methods	$q_{\text{max}}$ ( $\text{mg g}^{-1}$ )	pH	Refs.
Cow bone AC	$\text{HNO}_3$	32.10	4.0	[54]
Sewage sludge AC	$\text{HNO}_3$	135.5	4.0	[16]
Polygonum orientale Linn AC	$\text{H}_3\text{PO}_4$	98.39	5.0	[55]
AC	Triethylenetetramine	51.90	5.0	[56]
Chitosan	$\text{CH}_3\text{COOH}$	17.54	7.0	[57]
Pine cone AC	$\text{H}_3\text{PO}_4$	27.53	5.2	[58]
Coconut AC	$\text{H}_2\text{O}_2$	28.46	3.2–3.6	[59]
Bagasse MC	Ethylenediamine	185	4.5	This study

Table 8  
Pb(II) adsorption capacities of I7-EDA for three real water samples

Initial concentration $c_0$ (mg L <sup>-1</sup> )	Adsorption capacity (mg g <sup>-1</sup> )		
	Ultrapure water	Tap water	River water
5	4.98	4.73	4.43
10	9.96	9.65	9.38
30	29.47	26.17	23.21
50	49.72	46.57	41.32
100	98.59	91.23	87.36

I7-EDA are similar with the results of chitosan/graphene oxide composites and superabsorbent resin composite for the uptake of Pb(II) in previous studies [52,53]. This finding indicates excellent adsorption stability and broad application prospect.

### 3.9. Comparison of I7-EDA adsorbent performance with literature data

The maximum adsorption amount ( $q_{\max}$ ) of I7-EDA was compared with the adsorption capacities of Pb<sup>2+</sup> reported in the literature for other modified biomass adsorbents (Table 7). A direct comparison between the examined modified I7-EDA with those obtained in the literature was difficult because of the varying experimental conditions employed in the studies. However, the maximum adsorption amount  $q_{\max}$  values differ widely for different adsorbents (Table 7). Comparison of  $q_{\max}$  values showed that the adsorption capacity of I7-EDA prepared in our work was generally higher than previously reported values [16,54–59]. The high adsorption efficiency of I7-EDA may be attributed to the involvement of functional groups in both amino groups and MC I7 (synergistic effect). This result shows that I7-EDA is a potential candidate for applications in lead removal from contaminated water.

### 3.10. Application in real water samples

Three different water samples were applied to investigate the actual application of I7-EDA. Specifically, 0.100 g of I7-EDA was added into 100 mL of different initial concentrations of Pb(II) at 150 rpm and 25°C for 24 h for the adsorption test. The Pb(II) adsorption capacities of I7-EDA under three real water samples are shown in Table 8. The adsorption capacities toward Pb(II) in tap water and river water were slightly lower than ultrapure water because of numerous cations, such as Na<sup>+</sup>, K<sup>+</sup>, Ca<sup>2+</sup>, and Mg<sup>2+</sup> in tap and river water samples. These cations not only influenced ionic strength, aggrandizing the contact diffi-

culty between Pb(II) and I7-EDA, but also occupied the adsorption sites. However, I7-EDA maintains considerable adsorption capacity for Pb(II) ions in real water samples.

## 4. Conclusions

In this study, a cost-effective biomass-based MC with high Pb(II) adsorption performance was successfully synthesized from bagasse via microwave-assisted H<sub>3</sub>PO<sub>4</sub> activation, nitric acid oxidation, and ethylenediamine polymerization. The physicochemical analysis data indicated that the modified carbon I7-EDA was successfully functionalized with amino groups and maintained a mesoporous structure. The Pb(II) adsorption capacity was significantly enhanced after modification, and the adsorption behavior was well described by the Redlich–Peterson and Temkin isotherm models. This result implied that energy distribution was inhomogeneous on the I7-EDA surface. The pseudo-second-order kinetics model is the most appropriate to fit the adsorption kinetics data. The adsorption of Pb(II) was highly pH-dependent, and the highest adsorption capacity was obtained at a wide pH range of 5.0–8.0. In addition, the rate of Pb(II) adsorption on I7-EDA was rapid, and more than 70% of the ions were adsorbed within 5 min. The adsorption rate was mainly affected by intra-particle diffusion in the first stage. I7-EDA obtained also showed good durability, easy regeneration, and high removal efficiency of Pb(II) in real water samples. The XPS spectra before and after adsorption shows the amino groups combined with Pb(II) through strong complexation. Overall, this study demonstrated that the bagasse MC is a suitable precursor for preparation of amino-rich mesoporous material with significant adsorptive performance to Pb(II) ions.

## Acknowledgements

The authors gratefully acknowledge the research grant provided by China under the Natural Science

Foundation (No. 51102136), the Doctoral fund of Ministry of Education of China (No. 20110097120021), and the China Postdoctoral Science Fund (No. 2014M560429).

## References

- [1] Y. Motarjemi, Public health measures: Modern approach to food safety management: An overview, in: Y. Motarjemi (Ed.), *Encyclopedia of Food Safety*, Academic Press, Waltham, 2014, pp. 1–12.
- [2] H.K. Chung, Y.S. Chang, C.W. Ahn, Effects of blood lead levels on airflow limitations in Korean adults: Findings from the 5th KNHNES 2011, *Environ. Res.* 136 (2015) 274–279.
- [3] P. Chand, A. Bafana, Y.B. Pakade, Xanthate modified apple pomace as an adsorbent for removal of Cd(II), Ni(II) and Pb(II), and its application to real industrial wastewater, *Int. Biodeterior. Biodegrad.* 97 (2015) 60–66.
- [4] M.H. Mahaninia, P. Rahimian, T. Kaghazchi, Modified activated carbons with amino groups and their copper adsorption properties in aqueous solution, *Chin. J. Chem. Eng.* 23 (2015) 50–56.
- [5] L. Mao, H. Cui, H. An, B. Wang, J. Zhai, Y. Zhao, Q. Li, Stabilization of simulated lead sludge with iron sludge via formation of  $PbFe_{12}O_{19}$  by thermal treatment, *Chemosphere* 117 (2014) 745–752.
- [6] J. Zhu, J. Yang, B. Deng, Enhanced mercury ion adsorption by amine-modified activated carbon, *J. Hazard. Mater.* 166 (2009) 866–872.
- [7] W. Liu, J. Zhang, C. Zhang, Y. Wang, Y. Li, Adsorptive removal of Cr(VI) by Fe-modified activated carbon prepared from *Trapa natans* husk, *Chem. Eng. J.* 162 (2010) 677–684.
- [8] Z. Wang, C. Ye, X. Wang, J. Li, Adsorption and desorption characteristics of imidazole-modified silica for chromium (VI), *Appl. Surf. Sci.* 287 (2013) 232–241.
- [9] R. Yang, K.B. Aubrecht, H. Ma, R. Wang, R.B. Grubbs, B.S. Hsiao, B. Chu, Thiol-modified cellulose nanofibrous composite membranes for chromium (VI) and lead (II) adsorption, *Polymer* 55 (2014) 1167–1176.
- [10] Y. Wu, H. Luo, H. Wang, C. Wang, J. Zhang, Z. Zhang, Adsorption of hexavalent chromium from aqueous solutions by graphene modified with cetyltrimethylammonium bromide, *J. Colloid Interface Sci.* 394 (2013) 183–191.
- [11] H. Tamai, K. Shiraki, T. Shiono, H. Yasuda, Surface functionalization of mesoporous and microporous activated carbons by immobilization of diamine, *J. Colloid Interface Sci.* 295 (2006) 299–302.
- [12] R. Guo, J. Guo, F. Yu, D.D. Gang, Synthesis and surface functional group modifications of ordered mesoporous carbons for resorcinol removal, *Microporous Mesoporous Mater.* 175 (2013) 141–146.
- [13] G. Zeng, Y. Liu, L. Tang, G. Yang, Y. Pang, Y. Zhang, Y. Zhou, Z. Li, M. Li, M. Lai, X. He, Y. He, Enhancement of Cd(II) adsorption by polyacrylic acid modified magnetic mesoporous carbon, *Chem. Eng. J.* 259 (2015) 153–160.
- [14] T. Zhu, Y. Lu, S. Zheng, Y. Chen, H. Guo, Influence of nitric acid activation on structure and capacitive performances of ordered mesoporous carbon, *Electrochim. Acta* 152 (2015) 456–463.
- [15] Q. Li, G.-S. Ji, Y.-B. Tang, X.-D. Gu, J.-J. Fei, H.-Q. Jiang, Ultrasound-assisted compatible *in situ* hydrolysis of sugarcane bagasse in cellulase-aqueous-N-methylmorpholine-N-oxide system for improved saccharification, *Bioresour. Technol.* 107 (2012) 251–257.
- [16] H.-C. Tao, H.-R. Zhang, J.-B. Li, W.-Y. Ding, Biomass based activated carbon obtained from sludge and sugarcane bagasse for removing lead ion from wastewater, *Bioresour. Technol.* 192 (2015) 611–617.
- [17] P.L. Homagai, K.N. Ghimire, K. Inoue, Adsorption behavior of heavy metals onto chemically modified sugarcane bagasse, *Bioresour. Technol.* 101 (2010) 2067–2069.
- [18] L.H. Velazquez-Jimenez, A. Pavlick, J.R. Rangel-Mendez, Chemical characterization of raw and treated agave bagasse and its potential as adsorbent of metal cations from water, *Ind. Crops Prod.* 43 (2013) 200–206.
- [19] M. Wu, Q. Guo, G. Fu, Preparation and characteristics of medicinal activated carbon powders by  $CO_2$  activation of peanut shells, *Powder Technol.* 247 (2013) 188–196.
- [20] F. Raposo, M.A. De La Rubia, R. Borja, Methylene blue number as useful indicator to evaluate the adsorptive capacity of granular activated carbon in batch mode: Influence of adsorbate/adsorbent mass ratio and particle size, *J. Hazard. Mater.* 165 (2009) 291–299.
- [21] C.T. Hsieh, W.S. Fan, W.Y. Chen, Impact of mesoporous pore distribution on adsorption of methylene blue onto titania nanotubes in aqueous solution, *Micropor. Mesopor. Mat.* 116 (2008) 677–683.
- [22] A.N.A. El-Hendawy, Variation in the FTIR spectra of a biomass under impregnation, carbonization and oxidation conditions, *J. Anal. Appl. Pyrol.* 75 (2006) 159–166.
- [23] A.P. Terzyk, The influence of activated carbon surface chemical composition on the adsorption of acetaminophen (paracetamol) *in vitro*: Part II. TG, FTIR, and XPS analysis of carbons and the temperature dependence of adsorption kinetics at the neutral pH. *Colloids Surf. A* 177 (2001) 23–45.
- [24] W. Peng, Z. Xie, G. Cheng, L. Shi, Y. Zhang, Amino-functionalized adsorbent prepared by means of Cu(II) imprinted method and its selective removal of copper from aqueous solutions, *J. Hazard. Mater.* 294 (2015) 9–16.
- [25] Z. Zhang, F. Wang, W. Yang, Z. Yang, A. Li, A comparative study on the adsorption of 8-amino-1-naphthol-3,6-disulfonic acid by a macroporous amination resin, *Chem. Eng. J.* 283 (2016) 1522–1533.
- [26] J. Chen, Y. Zhai, H. Chen, C. Li, G. Zeng, D. Pang, P. Lu, Effects of pretreatment on the surface chemistry and pore size properties of nitrogen functionalized and alkylated granular activated carbon, *Appl. Surf. Sci.* 263 (2012) 247–253.
- [27] M.H. Kasnejad, A. Esfandiari, T. Kaghazchi, N. Asasian, Effect of pre-oxidation for introduction of nitrogen containing functional groups into the structure of activated carbons and its influence on Cu(II) adsorption, *J. Taiwan. Inst. Chem. Eng.* 43 (2012) 736–740.
- [28] J.P. Boudou, P. Parent, F. Suárez-García, S. Villar-Rodil, A. Martínez-Alonso, J.M.D. Tascón, Nitrogen in aramid-based activated carbon fibers by TPD, *Carbon* 44 (2006) 2452–2462.

- [29] R.J.J. Jansen, H. van Bekkum, XPS of nitrogen-containing functional groups on activated carbon, *Carbon* 33 (1995) 1021–1027.
- [30] H. Li, D.I. Xiao, H. He, R. Lin, P.I. Zuo, Adsorption behavior and adsorption mechanism of Cu(II) ions on amino-functionalized magnetic nanoparticles, *Trans. Nonferrous Met. Soc. China* 23 (2013) 2657–2665.
- [31] X. Xu, B.Y. Gao, X. Tan, Q.Y. Yue, Q.Q. Zhong, Q. Li, Characteristics of amine-crosslinked wheat straw and its adsorption mechanisms for phosphate and chromium (VI) removal from aqueous solution, *Carbohydr. Polym.* 84 (2011) 1054–1060.
- [32] M. Machida, R. Yamazaki, M. Aikawa, H. Tatsumoto, Role of minerals in carbonaceous adsorbents for removal of Pb(II) ions from aqueous solution, *Sep. Purif. Technol.* 46 (2005) 88–94.
- [33] H. Liu, P. Dai, J. Zhang, C. Zhang, N. Bao, C. Cheng, L. Ren, Preparation and evaluation of activated carbons from lotus stalk with trimethyl phosphate and tributyl phosphate activation for lead removal, *Chem. Eng. J.* 228 (2013) 425–434.
- [34] M. Jahangiri, F. Kiani, H. Tahermansouri, A. Rajabalinezhad, The removal of lead ions from aqueous solutions by modified multi-walled carbon nanotubes with 1-isatin-3-thiosemicarbazone, *J. Mol. Liq.* 212 (2015) 219–226.
- [35] Y. Tang, S. Liang, J. Wang, S. Yu, Y. Wang, Amino-functionalized core-shell magnetic mesoporous composite microspheres for Pb(II) and Cd(II) removal, *J. Environ. Sci.* 25 (2013) 830–837.
- [36] S. Wang, K. Wang, C. Dai, H. Shi, J. Li, Adsorption of Pb<sup>2+</sup> on amino-functionalized core-shell magnetic mesoporous SBA-15 silica composite, *Chem. Eng. J.* 262 (2015) 897–903.
- [37] Langmuir, The adsorption of gases on plane surfaces of glass mica and platinum, *J. Am. Chem. Soc.* 40 (1918) 361–1403.
- [38] F.H.M. Freundlich, Over the adsorption in solution, *J. Phys. Chem.* 57 (1906) 385–471.
- [39] T.M.V. Pyzhev, Kinetics of ammonia synthesis on promoted iron catalysts, *Acta Physicochim. URSS*, 12 (1940) 327–356.
- [40] O. Redlich, D.L. Peterson, A useful adsorption isotherm, *J. Phys. Chem.* 63 (1959) 1024–1026.
- [41] F.C. Wu, R.L. Tseng, R.-S. Juang, Characteristics of Elovich equation used for the analysis of adsorption kinetics in dye-chitosan systems, *Chem. Eng. J.* 150 (2009) 366–373.
- [42] T. Akkaya, M. Gülfen, U. Olgun, Adsorption of rhodium (III) ions onto poly(1,8-diaminonaphthalene) chelating polymer: Equilibrium, kinetic and thermodynamic study, *React. Funct. Polym.* 73 (2013) 1589–1596.
- [43] H. Javadian, M. Taghavi, Application of novel Polypyrrole/thiol-functionalized zeolite Beta/MCM-41 type mesoporous silica nanocomposite for adsorption of Hg<sup>2+</sup> from aqueous solution and industrial wastewater: Kinetic, isotherm and thermodynamic studies, *Appl. Surf. Sci.* 289 (2014) 487–494.
- [44] S.K. Singh, T.G. Townsend, D. Mazyck, T.H. Boyer, Equilibrium and intra-particle diffusion of stabilized landfill leachate onto micro- and meso-porous activated carbon, *Water Res.* 46 (2012) 491–499.
- [45] A.L. Srivastav, P.K. Singh, V. Srivastava, Y.C. Sharma, Application of a new adsorbent for fluoride removal from aqueous solutions, *J. Hazard. Mater.* 263, Part 2 (2013) 342–352.
- [46] Z. Ali, A. Khan, R. Ahmad, The use of functionalized aerogels as a low level chromium scavenger, *Micropor. Mesopor. Mat.* 203 (2015) 8–16.
- [47] C.K. Lee, L.H. Lai, S.S. Liu, F.C. Huang, H.-P. Chao, Application of titanate nanotubes for ammonium adsorptive removal from aqueous solutions, *J. Taiwan. Inst. Chem. Eng.* 45 (2014) 2950–2956.
- [48] F.C. Wu, R.L. Tseng, R.S. Juang, Initial behavior of intraparticle diffusion model used in the description of adsorption kinetics, *Chem. Eng. J.* 153 (2009) 1–8.
- [49] S. Shen, T. Pan, X. Liu, L. Yuan, J. Wang, Y. Zhang, Z. Guo, Adsorption of Rh(III) complexes from chloride solutions obtained by leaching chlorinated spent automotive catalysts on ion-exchange resin Diaion WA21 J, *J. Hazard. Mater.* 179 (2010) 104–112.
- [50] P. Castaldi, M. Silvetti, G. Garau, D. Demurtas, S. Deiana, Copper (II) and lead (II) removal from aqueous solution by water treatment residues, *J. Hazard. Mater.* 283 (2015) 140–147.
- [51] J. Chung, J. Chun, J. Lee, S.H. Lee, Y.J. Lee, S.W. Hong, Sorption of Pb(II) and Cu(II) onto multi-amine grafted mesoporous silica embedded with nanomagnetite: Effects of steric factors, *J. Hazard. Mater.* 239–240 (2012) 183–191.
- [52] L. Fan, C. Luo, M. Sun, X. Li, H. Qiu, Highly selective adsorption of lead ions by water-dispersible magnetic chitosan/graphene oxide composites, *Colloid. Surface.* 103 (2013) 523–529.
- [53] Q. Li, H. Lu, H. Xiao, K. Gao, M. Diao, Adsorption capacity of superabsorbent resin composite enhanced by non-thermal plasma and its adsorption kinetics and isotherms to lead ion in water, *J. Environ. Chem. Eng.* 1 (2013) 996–1003.
- [54] M.A.P. Cechinel, S.M.A. G. Ulson de Souza, A.A. Ulson de Souza, Study of lead (II) adsorption onto activated carbon originating from cow bone, *J. Clean. Prod.* 65 (2014) 342–349.
- [55] L. Wang, J. Zhang, R. Zhao, Y. Li, C. Li, C. Zhang, Adsorption of Pb(II) on activated carbon prepared from *Polygonum orientale* Linn: Kinetics, isotherms, pH, and ionic strength studies, *Bioresour. Technol.* 101 (2010) 5808–5814.
- [56] L. Zhang, X. Chang, Z. Li, Q. He, Selective solid-phase extraction using oxidized activated carbon modified with triethylenetetramine for preconcentration of metal ions, *J. Mol. Struct.* 964 (2010) 58–62.
- [57] V. Manasi, N. Rajesh, An indigenous *Halomonas* BVR1 strain immobilized in crosslinked chitosan for adsorption of lead and cadmium, *Int. J. Biol. Macromol.* 79 (2015) 300–308.
- [58] M. Momčilović, M. Purenović, A. Bojić, A. Zarubica, M. Randelović, Removal of lead(II) ions from aqueous solutions by adsorption onto pine cone activated carbon, *Desalination* 276 (2011) 53–59.
- [59] X. Song, H. Liu, L. Cheng, Y. Qu, Surface modification of coconut-based activated carbon by liquid-phase oxidation and its effects on lead ion adsorption, *Desalination* 255 (2010) 78–83.